Ceramics International 46 (2020) 10820–10828

Contents lists available at ScienceDirect

Ceramics International

journal homepage: www.elsevier.com/locate/ceramint

Optical, electrical and magnetic properties of copper doped electrodeposited MoO_3 thin films

Rufus O. Ijeh[a,b], Assumpta C. Nwanya[b,c,d], Agnes C. Nkele[b], Itani G. Madiba[c,d], A.K.H. Bashir[c,d], A.B.C. Ekwealor[b], R.U. Osuji[b,c,d], M. Maaza[c,d], Fabian Ezema[b,c,d,e,*]

[a] Science Education Department, College of Education, Agbor, Nigeria
[b] Physics and Astronomy Department, University of Nigeria, Nsukka, Nigeria
[c] Nanosciences African Network (NANOAFNET) iThemba LABS-National Research Foundation, 1 Old Faure Road, Somerset West 7129, P.O. Box 722, Somerset West, Western Cape Province, South Africa
[d] UNESCO-UNISA Africa Chair in Nanosciences/Nanotechnology, College of Graduate Studies, University of South Africa (UNISA), Muckleneuk Ridge, P. O. Box 329, Pretoria, South Africa
[e] Department of Physics, Faculty of Natural and Applied Sciences, Coal City University, Enugu, Nigeria

ARTICLE INFO

Keywords:
Electrodeposition
Cu-doped MoO_3
Orthorhombic
Doping
Band gap

ABSTRACT

Copper-doped MoO_3 thin films were prepared via electrodeposition technique. The techniques adopted for investigating the structural, optical, electrical and magnetic properties of both undoped and copper-doped MoO_3 thin films include X-ray diffractometry, UV–visible spectroscopy, four-point probe and vibrating sample magnetometry respectively. Nanocrystalline homogenous grains with polycrystalline orthorhombic (α-MoO_3) nature were obtained. The optical plots recorded decreased band gap energy from 3.44 eV to 3.27 eV, magnetic studies showed ferromagnetic properties of the doped samples while the electrical study revealed the highest conductivity of 1.5 Ωcm^{-1}. Doping with Cu has the potentiality of increasing the conductivity of MoO_3 thereby enhancing its application in photocells.

1. Introduction

Molybdenum trioxide (MoO_3) is an important transition metal oxide that has attracted the attention of researchers. It portrays a high degree of fascinating optical and electrical properties as a result of its notable technological applications [1–6]. MoO_3 is a wide n-type semiconductor ($E_{g'}$ = 3.1 eV) with high ionic conductivity as a result of oxygen vacancies [7]. The three stages of molybdenum trioxide include monoclinic (β-MoO_3), hexagonal (h-MoO_3) and orthorhombic (α-MoO_3) with the later having the highest stability [8]. The layered structure makes its' absorption of light readily and uniformly available for responses in electrochromic and photochromic displays [4]. These properties enhance its applications in smart windows [9], light emitting diodes [10], optical switching coatings [11], gas sensors [12,13] and lithium batteries [2,7]. Recently due to the interest in spintronic devices, a lot of researches are focused on doping non-magnetic semiconductors with Li, Cu, Mn in order to produce semiconductors with ferromagnetic properties. Doping causes electrons to become unpaired and enables researchers to exploit the properties of materials in order to modulate the transport of electrons and holes in semiconductors [14,15]. It is obvious that the conductivity in most transition metal oxide thin films is due to the oxygen vacancies and available free carriers [16–19]. It is also of importance to know that the value of resistivity of a semiconductor is a prominent factor in determining its' conductivity. To some degree; doping enhances the magnetic, optical and electrical properties of materials; thereby resulting in greater efficiency, better stability, and higher speed. Antiferromagnetic materials exhibit zero net magnetic moments in zero applied fields although smooth particles of the same material could be superparamagnetic or exhibit weak ferromagnetism [20]. It is worthy of note that different methods that were adopted by researchers for depositing MoO_3 thin films include spray pyrolysis [21,22], sol-gel method [23], chemical vapour deposition [24,25], chemical bath deposition [26–28], pulsed laser deposition [29–32], magnetron sputtering [33,34] and mussel-inspired chemistry [35,36]. We decided to adopt electrochemical deposition technique in this work after critical examinations of other deposition techniques for the synthesis of copper doped molybdenum as it has potent industrial applications due to its prominent purity which helps the films to be processed and grown at room temperature [37]. Rosalinda et al. electrodeposited and characterized molybdenum oxide and observed that the

* Corresponding author. Physics and Astronomy Department, University of Nigeria, Nsukka, Nigeria.
E-mail address: fabian.ezema@unn.edu.ng (F. Ezema).

https://doi.org/10.1016/j.ceramint.2020.01.093
Received 4 December 2019; Received in revised form 5 January 2020; Accepted 10 January 2020
Available online 16 January 2020

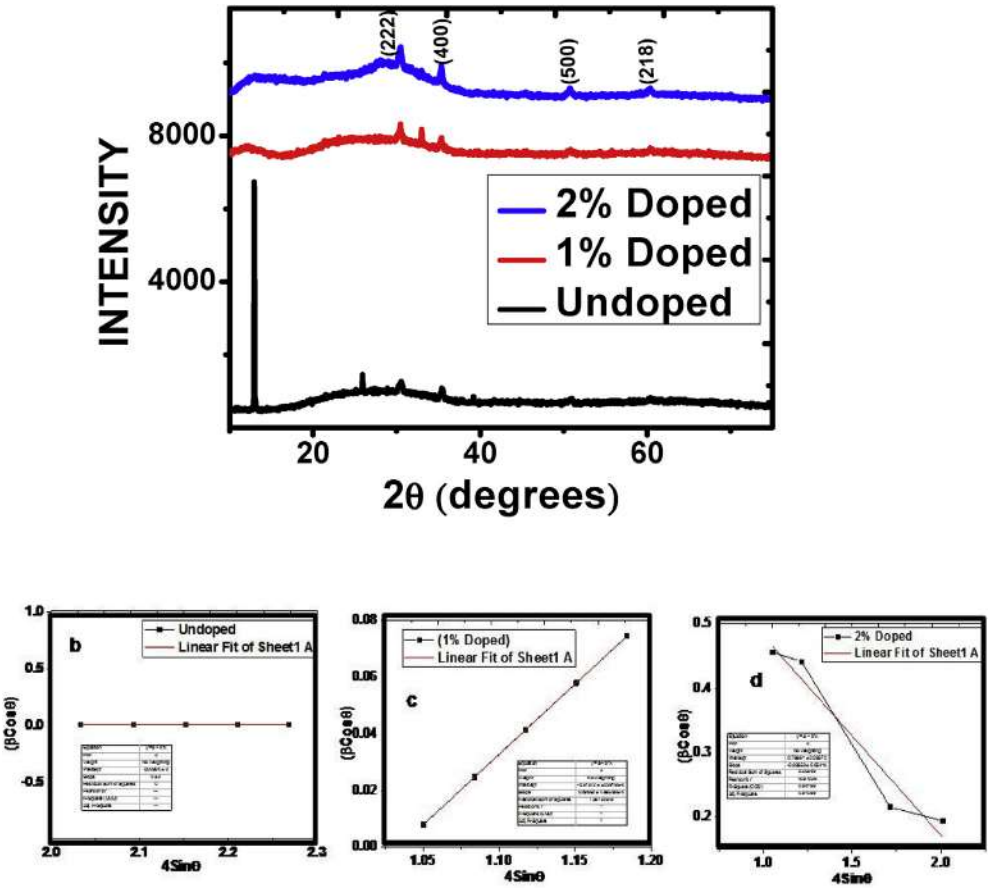

Fig. 1. (a) Structural patterns of the MoO_3 thin films, (b-d}Williamson-Hall (W–H) Plots of the deposited films.

nanostructures were amorphous with its morphology changing with pH. The optical band gap was of direct nature with a value of 3.2 eV [38]. Boukhachem et al. [21] synthesized cobalt doped MoO_3 using spray pyrolysis and the films showed orthorhombic structure with grain sizes in the range of 150–280 nm. The magnetic investigation showed that the films exhibited ferromagnetic behaviour. Seyyed and Mohammad doped h-MoO_3 thin films with Zn using a hydrothermal technique. The optical studies showed that the seed layer had increasing band gap energy from 3.2 eV to 3.54 eV [4]. Gesheva et al. successfully prepared MoO_3 thin films via chemical vapour deposition method. The transmittance of the films was 80% and the index of refraction ranged at 1.55 with 3.5 eV as the band gap energy [4]. Bouzidi et al. studied temperature effect on the optical properties of MoO_3 films using a spray pyrolysis technique. The films prepared at 200 °C were found to have orthorhombic structure, polycrystalline nature and energy band gap between 3.14 eV and 3.34 eV [1]. Boukhachem et al. prepared undoped and tin (Sn) doped (α-MoO_3) thin films via spray pyrolysis. They found that by increasing the amount of dopant; dense nano-platelet was formed, transmittance increased to 50% and band gap energy increased to 3.89 eV [22]. Han-Yi Chen et al. investigated indium-doped molybdenum oxide thin films and found the films to exhibit high optical transmittance of about 88% with low resistivity which makes it germane for applications in photovoltaic device [9]. The desire for this work arose due to the increased resistivity of intrinsic molybdenum trioxide [39]. Hence our interest is based on doping molybdenum trioxide with copper to enhance the conductivity of MoO_3 as there exists no literature yet on it. Therefore this research work adopted the electrodeposition method in studying the morphological, optical, magnetic and electrical properties of the undoped and copper-doped molybdenum trioxide thin films.

2. Experimental procedures

2.1. Materials

Indium-doped tin oxide (ITO) substrate, sodium hydroxide (NaOH), ammonium molybdate tetrahydrate $(NH_4)_6Mo_4O_{24}.4H_2O$, copper sulphate pentahydrate solution ($CuSO_4.5H_2O$), platinum mesh, silver-silver chloride (Ag/AgCl) electrode.

2.2. Synthesis

Electrochemical deposition was adopted in synthesizing undoped and doped MoO_3 thin films. The ITO coated substrate which served as the working electrode was cut into dimensions of 2.5 cm × 1.5 cm and soaked in detergent. Thereafter, the substrates were rinsed in de-ionized water and cleansed in acetone for 30 min in order to remove the grease that can inhibit nucleation and growth of thin films. For the preparation of MoO_3 nanoparticles, 100 ml of 1 M NaOH was mixed with 80 ml of 0.55 M of ammonium molybdate tetrahydrate $(NH_4)_6Mo_4O_{24}.4H_2O$ aqueous solution. To prepare the copper dopant, 1 and 2 wt% of copper sulphate pentahydrate solution ($CuSO_4.5H_2O$) was added to 80 ml of 0.55 M of ammonium molybdate tetrahydrate ($(NH_4)_6Mo_4O_{24}.4H_2O$). The pH was regulated to 10 using NaOH as a precipitator agent. The chamber consists of three-electrode configuration: platinum mesh as the anode, working electrode as the cathode, silver-silver chloride (Ag/AgCl) as a reference electrode. ITO coated substrate was placed vertically erect into the chamber containing the counter and reference electrodes for each deposition. The deposition was carried out under a potentiostatic condition of −200 mV vs SCE for 10 min. The deposited films were consequently cleaned and dried using the hand drier. The films were then transferred to a high-temperature

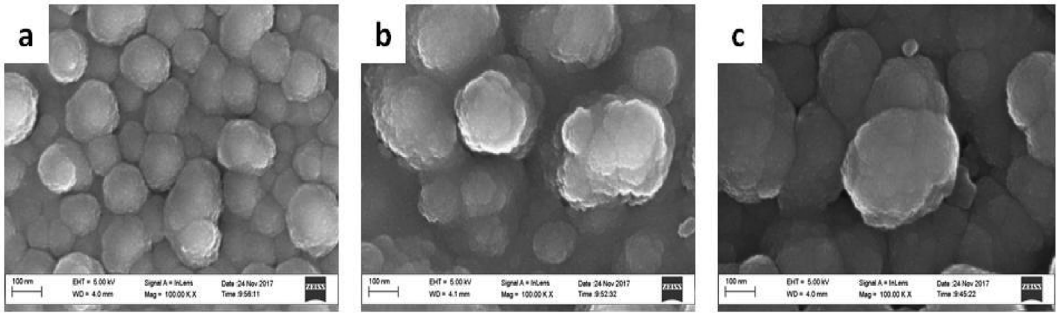

Fig. 2. SEM images of a) undoped and b-c) MoO_3:Cu thin films.

furnace for heat treatment at 373 K for 1 h. Gravimetric method was employed in measuring the film thicknesses using equation (1) [40]:

$$\text{Thickness} = \text{mass difference} / (\text{area of deposit x density}) \quad (1)$$

The mass differences of the undoped, 1% and 2% doped samples were obtained to be 0.0008 g, 0.0006 g and 0.0005 g respectively with its respective thicknesses being 935.9 nm, 702.0 nm and 584.9 nm.

2.3. Characterization

The X-ray diffraction analysis (PHILIPS-PW3710) and SEM model JSM 35 CFJEOL were respectively used for the structural and morphological studies of the undoped and copper-doped molybdenum trioxide thin films. The resistivity measurements were embarked upon using a four-point probe meter in which current and voltage readings were recorded. The magnetization readings were also recorded using vibrating sample magnetometer (VSM) [Lake Shore Model 7404].

3. Results and discussion

3.1. Structural studies

The structural patterns of the undoped and copper-doped MoO_3 thin films deposited on ITO substrates via electrochemical technique is shown in Fig. 1(a). It is evident that the undoped and the doped thin films exhibit peaks diffracted at $2\theta = 30.0^{\circ}$, 35.3°, 50.0°, and 62.8° assigned to the (222), (400), (500) and (218) crystal planes respectively and correspond to the polycrystalline phase in nature. Furthermore, all peaks identified are indexed as orthorhombic structure (PDF card no.00-047-1320) as no other similar compounds were grown. There is evidence of the strong intensity of the reflection peaks at (222) and (400) of both undoped and doped MoO_3 nanoparticles which are consistent with the works of Elangovan et al. [41]. The strongest reflection from (222) orientation is observed for the 2% doped sample showing the dopant effect on MoO_3 thin films. Fig.1(a) shows the XRD of undoped and MoO_3: Cu thin films with Cu-Kα radiation at wavelength, $\lambda = 1.54056$ Å, and diffraction angle between 20° and 75°. The crystallite size was also calculated using Williamson-Hall equation as in equation (2) [42]:

$$\beta\cos\theta = k\lambda/D + 4\varepsilon\sin\theta \quad (2)$$

where β is the full width at half maximum (FWHM), θ is the radian angle, k has a constant value 0.9, ε is the strain and λ is the X-ray wavelength from Cu-K_α at 1.5406 Å. This can be compared to the standard equation for a straight line

$$y = mx + c \quad (3)$$

where m is the slope and c is the intercept. By plotting βcosθ versus 4sinθ as shown in Fig. 1(b–d), straight-line graphs were obtained for each sample.

From the linear fitting; the slopes and intercepts were used to obtain the strain and crystal sizes respectively as contained in Fig. 1(b–d). It was discovered that the undoped sample shown in Fig. 1(b) had intercept of 0.00824 with zero slope. This indicates a very small crystal size with an absence of strain in the crystal lattice. Furthermore, the 1% doped sample has an intercept of −0.513 with a slope of 0.496 while the 2% doped has intercept of 0.7886 with −0.30853 slope. This shows that the more the percentage of the dopant, the greater the crystallite size. However, the negative slopes observed indicate insignificant values of strain broadening within the lattice and shift towards higher angles [43,44]. This result agrees with the works of Yousefi et al. [45] as regards the grain size increasing with percentage doping. The lattice strain, ε produced by disparity due to the introduction of Cu^+ into the MoO_3 lattice is given by equation (4) [45]:

$$\varepsilon = \beta / 4\tan\theta \quad (4)$$

The calculated average values of stain using equation (4) for the 1% and 2% doped samples were 0.00431 and 0.00437 respectively. These insignificant values validate the Williamson-Hall plot method used in this work.

3.2. Morphological studies

The surface morphologies of the molybdenum trioxide thin films prepared at the same pH value at room temperature are seen in Fig. 2(a–c).

The undoped and doped nanoparticles are spherically shaped, homogeneously distributed without pinholes or cracks having almost regular sizes, shapes and cross-linked. It is also evidenced that the doped nanoparticles have larger sizes with some overgrown clusters compared with the undoped as seen in Fig. 2(b and c). Also, the 2% doped nanoparticles had the largest surface area showing densely overgrown areas than the undoped and 1% doped nanoparticles. The cluster formation of smaller grains which transformed into larger sizes could be due to nucleation of the particles on the substrates showing a more pronounced doping effect.

3.3. Optical studies

3.3.1. Optical absorbance and transmittance

The absorbance and transmittance spectra of the deposited films are observable in Fig. 3(a and b). Absorbance of the MoO_3: Cu thin films were found to decrease gradually within the visible region as the wavelength increased.

At 300 nm, the absorbance value for the undoped film ranged at 23.6% and gradually tended towards the infra-red region while the 1% doped MoO_3 thin films absorbed at 29.3% and was fairly constant within the visible region. Furthermore, the 2% copper doped recorded the highest absorbance and decreased exponentially thereby converging with the 1% doped and undoped thin films in the infra-red region as shown in Fig. 3(a). Optical absorption spectra of the films in the spectral region between 300 and 1000 nm were recorded with a

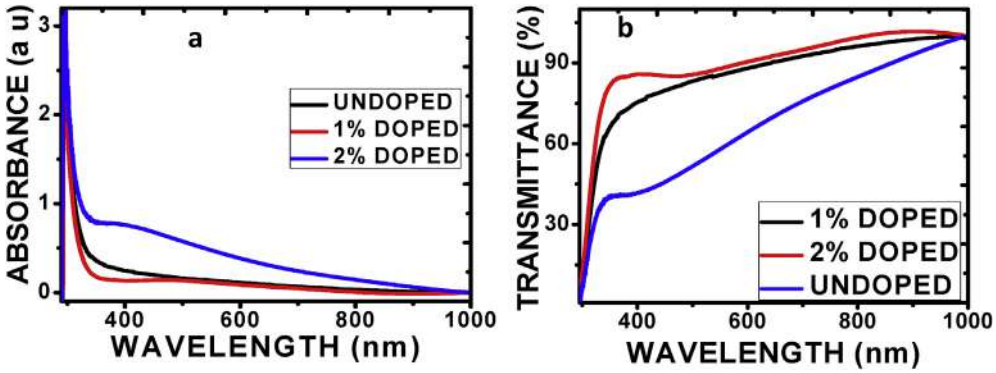

Fig. 3. a) Absorbance and b) Transmittance spectra for the undoped and doped MoO_3:Cu films.

UV–visible spectrophotometer.

From the transmittance spectrum in Fig. 3(b), all the thin films recorded increased transmittance at increasing wavelength. At 350 nm, the undoped film had the least transmittance at about 40% while the 1% and 2% doped films transmitted at 66.5% and 81.1% respectively. From the above, 2% doped thin film showed the maximum transmittance within the visible region. This result agrees with the work of Elangovan et al. [41]. The deposition parameters and texture of the thin films are germane to the determination of optical transmittance. The optical absorption coefficient, α was calculated using equation (5) [42]. It was observed that the undoped MoO_3 had the highest transmittance in the near infrared region which suggests that the material could be applicable for devices that can generate heat into a building [46].

$$\alpha = (1/d) \ln (1/T) \quad (5)$$

where *d is* sample thickness, and *T* is transmittance.

3.3.2. Optical band gap

Optical band gap energy values can be determined when absorbed electrons get excited from the valence band to conduction band. It has been established that near the UV, the band gap energy of MoO_3 can be used as a photochromic material [47]. A variation of absorption coefficient with the energy of photons seen in Fig. 4 is usually used in determining the optical band gap (E_g) of the thin films using equation (6).

The type of transition is determined by using Tauc's relation [48].

$$(\alpha h\nu)^2 = A(h\nu - E_g)^n \quad (6)$$

Where $h\nu$ is the photon energy, A is a constant called absorption coefficient, E_g is the band gap energy and n = 1/2 for allowed direct transition or 2 for indirect interband transitions. The optical band gap is obtained by extending the straight-line portion of the plot to meet the photon energy axis as shown in Fig. 4. The direct band gaps for the undoped MoO_3 thin film was 3.44 eV, 1% was 3.35 eV and 2% doped was 3.27 eV. This is similar to the works of Bouzidi et al. [1], Chibane et al. [32], Rosalinda et al. [38], Julien et al. [49] and Ganchev et al. [50]. Obviously, the energy band gap decreased with increase in percentage of copper dopant culminated from particle size increase as contained in Table 1. This decrease could be because of morphological, surface microstructure and particle size changes [42]. There exists a red-shift in the absorption edge for the samples at different Cu-dopant percentages. The band gap reduces with an increase in percentage doping as a result of capturing of electrons by oxygen vacancies and an increase in electron density which results in the distorting effect of the valence band and conduction band [51]. Copper atoms now serve as the center for the activation of scattering.

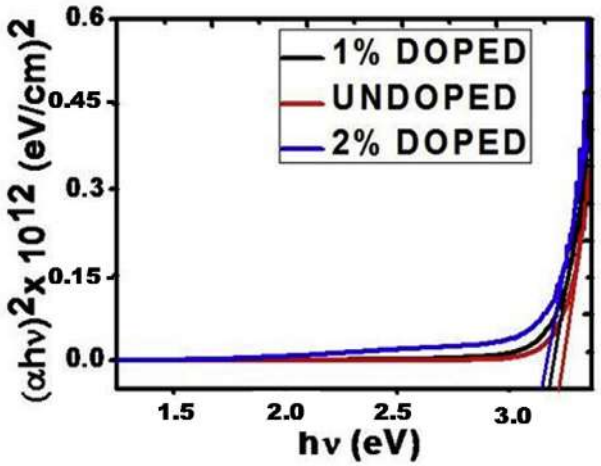

Fig. 4. Plot of optical band gaps of the undoped and doped MoO_3 thin films.

3.3.3. Refractive index

Fig. 5 represents changes in refractive indices as a function of wavelength of undoped MoO_3 and Cu-doped MoO_3thin films. The refractive index values were obtained using equation (7) [52]:

$$n = (1 + \text{sqrt } R) / (1 - \text{sqrt } R) \quad (7)$$

where *n* is the refractive index, R is reflectance.

The refractive index values rise sharply at low wavelength before peaking at 2.54 for the undoped, the 1% and 2% samples recorded peaks at 2.62 and 2.64 respectively. High refractive indices in the doped samples could be due to oxygen presence. The dopant effect was observed in the refractive index of the doped samples compared with the undoped as shown in Fig. 5. The refractive indices of the films had values ranging from 2.54 to 2.64 at increasing wavelength regions. It is noted that while Uthanna et al., Reyes-Betanzo et al., and Cardenas et al. obtained refractive index values of 1.8, 1.9 and 2.1 using thermal evaporation, pulsed laser and magnetron sputtered methods respectively; our result seems not to deviate much from the values obtained owing to the deposition technique employed [53–55].

3.3.4. Optical conductivity

Fig. 6 depicts the variation of optical conductivity for both undoped and MoO_3: Cu. The Optical conductivity, ρ, is defined in equation (8) [56]:

$$\rho = \alpha\eta c / 4\pi \quad (8)$$

where c is the speed of light, α is the absorption coefficient, and n is the refractive index.

The undoped sample showed the lowest conductance due to low energy density. We observed in Fig. 6 that the doped samples had a sharp increase in conductance at low photon energies. The high conductivity in the doped samples could be due to a strong interactive force

Table 1
Energy band gap, magnetization and electrical conductivity of samples.

Sample	Energy band gap (eV)	Magnetic saturation (M_s) (emu/g)	Coercive field (H_c) (O_e)	Electrical conductivity, σ $(\Omega\ cm)^{-1}$
Undoped	3.44	-3.87×10^{-4}	−0.50	−0.29
1% Doped	3.35	4.52×10^{-4}	42.35	−0.16
2% Doped	3.27	4.60×10^{-4}	49.12	1.50

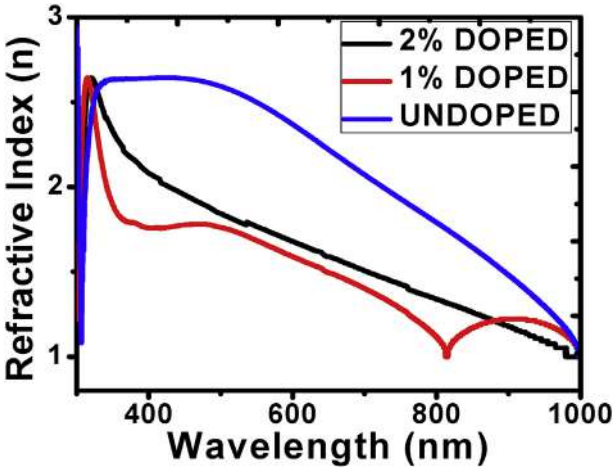

Fig. 5. Refractive indices of undoped and copper-doped MoO_3 thin films.

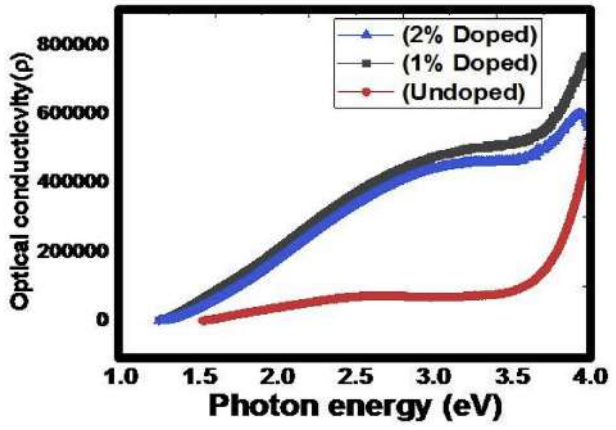

Fig. 6. Optical conductivity plot of undoped and MoO_3: Cu thin films.

between the photons and electrons [57]. The conductance of 2% doped sample was slightly lower than the 1% doped which might be due to deposition parameters. It is also observed that the conductance of the undoped sample increased fairly at higher photon energy. The optical conductivity of samples is dependent on the band gap and in this work, as the band gap decreased, the optical conductivity increased due to the introduction of charge carriers [58,59].

3.3.5. Extinction coefficient

It measures how light is thrown off by a material at any given wavelength. Extinction coefficient values can be obtained using equation (9) [60]:

$$k = \alpha\lambda / 4\pi \quad (9)$$

where k is the extinction coefficient, λ is wavelength of the incident photon, α is the absorption coefficient.

The increase in the extinction coefficient with photon energy is more pronounced for doped samples than the undoped as depicted in Fig. 7. This is due to the presence of Cu^+ in the molybdenum atom. The

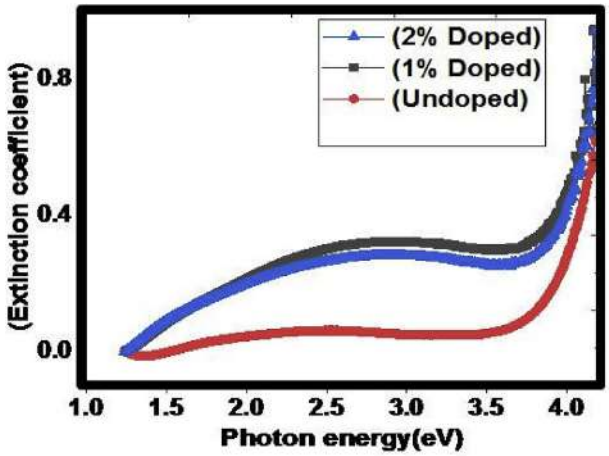

Fig. 7. Plot of the Extinction coefficient of MoO_3 thin films.

extinction coefficient of the undoped varies from 0.2 to 0.4 while the doped samples varied from 0.2 to 0.5.

3.3.6. Dielectric constants

The real and imaginary dielectric constants are obtained from the refractive index and extinction coefficient values. The measurement of how the speed of light decreases in a medium describes the real part while the imaginary designates the loss of energy to the medium. The values of ε_r and ε_i used for this work were calculated using the relations in equations (10) and (11) [61]:

$$\mathcal{E}_r = n^2 - k^2 \quad (10)$$

$$\mathcal{E}_i = 2nk \quad (11)$$

Fig. 8 (a,b) show the real and imaginary dielectric constants of both undoped and doped samples of MoO_3. The characteristics pattern for the real and dielectric constants differ as the real parts have higher values compared to the imaginary. The imaginary part increases sharply at lower photon energies and shrank at higher energies. The relaxation peaks of real and imaginary parts are 4.1 and 1.2 respectively.

3.4. Magnetic properties

The magnetic studies of undoped MoO_3 and copper doped MoO_3 samples have been carried out using the VSM technique. Plotting of the magnetic moment against the applied magnetic field as shown in Fig. 9 depicts the behavior of magnetism of both undoped MoO_3 and copper doped MoO_3 nanoparticles at room temperature.

There exist exchange interactions between the local spin-polarized electrons occasioned by the copper ions and excess conductive electrons of the MoO_3 resulting in the formation of the loop. The application of a magnetic field causes the unpaired spins yielding to some non-zero ferromagnetic moment [62]. From the M − H loop, it was noticed that the undoped MoO_3 depicts some elements of antiferromagnetic behavior as shown in Fig. 9(a) while the samples doped with copper exhibited ferromagnetic properties shown in Fig. 9(b). The evidence of ferromagnetic ordering is attributed to the high magnetizing nature of

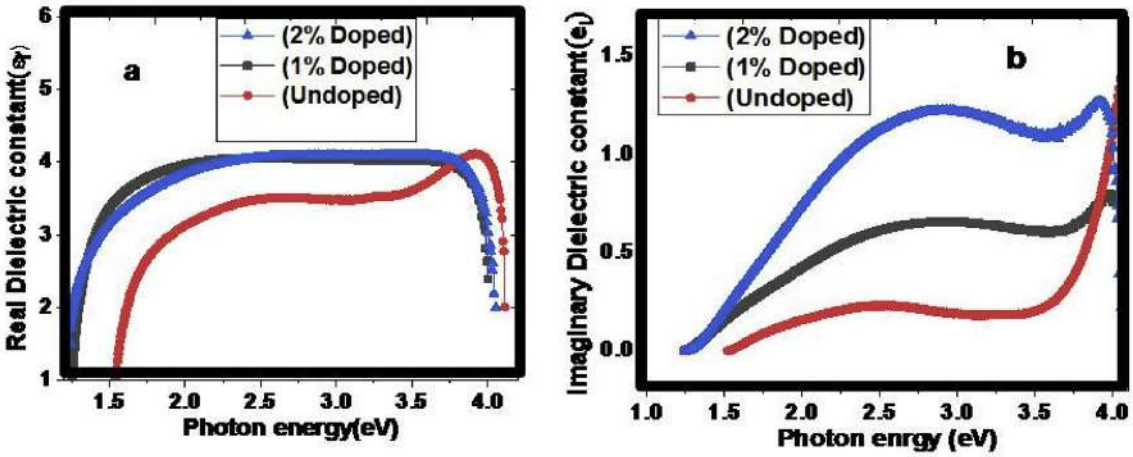

Fig. 8. (a & b): Plots of Dielectric constants of MoO_3 thin films.

Cu ions introduced into the Mo atom arranged in orthorhombic structure as magnetic element doping leads to the room temperature ferromagnetism [63–65]. In this work, we observed that an increase in both magnetization and coercive field values was due to the increase in grain size culminated from the addition of Cu ions as seen both in ferromagnetic ordering in Fig. 9(b). This also validates the literature on works of Shah et al., Gopalakrishnan et al. [66,67]. The saturation magnetization for the undoped is around -3.87×10^{-4} having a magnetic field of 1.49×10^{-4} and negative coercivity of -0.50 shown in Table 1. The copper doping of 1%wt in MoO_3 enhances the magnetization and coercivity with a value of 4.52×10^{-4} and 42.35 respectively while an increase in doping (2 %wt) culminated an increase in both magnetization and coercivity values of 4.60×10^{-4} and 49.12 respectively showing doping effect as contained in Table 1. This work is in concomitance with the study conducted by Godlyn et al. [68] and Ahmed et al. [69] which supports that the number of impurity ions introduced into the host atom increases both saturation magnetization and coercivity values. The increase in magnetization may be related to the presence of oxygen vacancies [70,71]. Also, the magnetic field for the 1% doped sample ranged between 1.48×10^{-4} and -1.75×10^{-4} while that for the 2% doped sample ranged between 4.56×10^{-4} and -4.67×10^{-4}.

3.5. Electrical properties

A four-point probe as schematically represented in Fig. 10(a) is a technique used for measuring the resistivity of semiconductor material

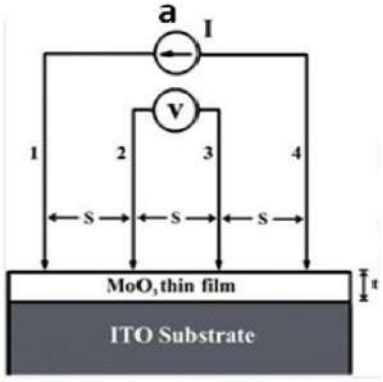

Fig. 10(a). Schematic diagram of Four Point Probe.

by ascertaining the opposition to the flow of charge carriers. Generally, the electrical resistivity is inversely proportional to the carrier density and carrier mobility [72]. The I–V data for the MoO_3 samples were used to obtain the conductivity of the thin films. The conductivity of a sample can be evaluated from the voltage-current relationship in equations (12) and (13):

$$\rho = 4.532\ (V/I)t = R_s t \quad (12)$$

$$\rho = 1/\delta \quad (13)$$

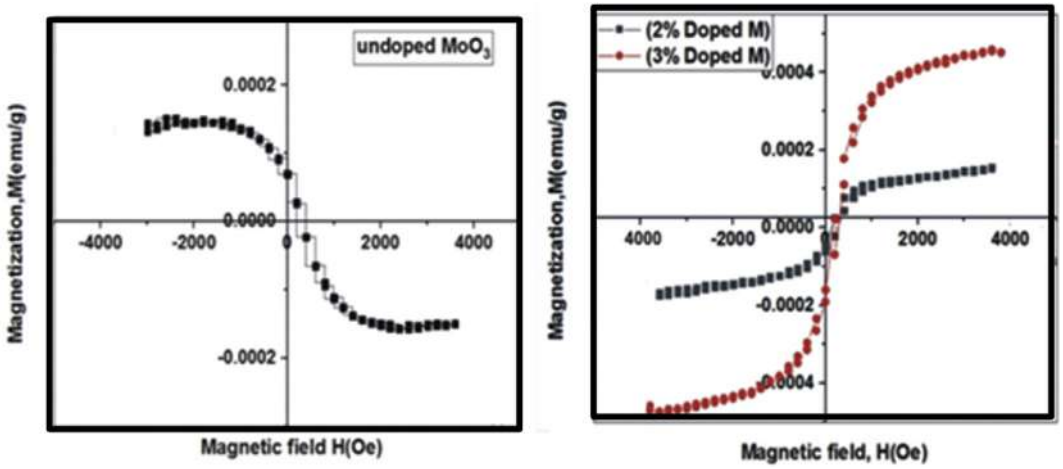

Fig. 9. (a): Variation of magnetic M − H curve of undoped MoO_3 sample (b): Variation of magnetic M − H curve of the doped MoO_3 thin samples.

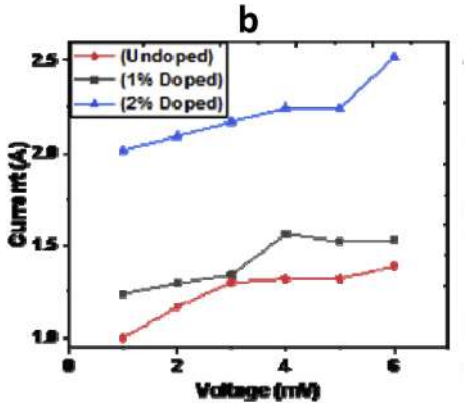

Fig. 10(b). Variation of voltage with current.

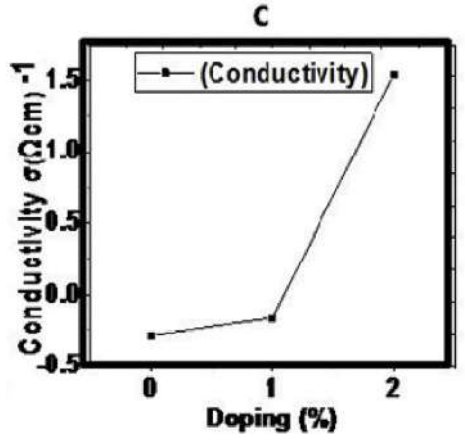

Fig. 10(c). Variation of conductivity with doping.

where V, I, ρ, R_s are the voltage, current, resistivity, sheet resistance, and t, the thickness of the film respectively.

The current is passed through the outer probes (1 and 4) while measurement of voltage occurs between the two inner probes (2 and 3) as shown in Fig. 10(a). It is observed in Fig. 10(b) that when the current was increased in the undoped sample, the recorded voltage remained fairly constant at 0. For the 1 and 2% doped samples, the voltage readings were negative at low current values. As the current increased further, the voltage increased to 2.0×10^{-4} V for 2% doped and dropped drastically due to the structural defects occasioned by grain boundaries and dislocations, leading to scattering and inhibition of carrier mobility. Beyond 20 A, the voltage increased to 1.83×10^{-4} and 3.62×10^{-4} for 1 and 2% doped respectively. Variation of electrical conductivity (σ) with doping percentage was investigated on both pure and Cu doped MoO_3 thin films at room temperature as shown in Fig. 10(c). There is a sharp increase in conductivity value for the 2% doped sample compared to the 1% doped and undoped sample denoted by 0%. The undoped sample recorded the least value as carrier density is very low. The result suggests that the addition of Cu improved the conducting properties of MoO_3 samples without altering other basic properties. The observed increase in electrical conductivity for higher percentage doping is due to the increase in carrier concentration introduced by Cu^{+2} cation and deposition parameter for the maintenance of charge neutrality [64]. Table 1 summarizes the measured values of the energy band gap, magnetic saturation, coercive field and electrical conductivity of the films.

4. Conclusions

A study of undoped and copper-doped MoO_3 was employed using the electrodeposition method. The crystallographic studies of both doped and undoped thin films revealed polycrystalline nature with an orthorhombic (α- MoO_3) structure. The surface morphology showed nanocrystalline grains that are spherically shaped, homogeneously distributed with grain sizes that increased with dopant percentages. The energy band gap decreased from 3.44 eV to 3.27 eV at increasing dopant percentages. The maximum transmittance value for the undoped and 1% doped thin films was 80% while the 2% doped thin film recorded 63% in the visible range. The optical conductivity plot affirms that the doped samples had higher conductivities than the undoped sample while ferromagnetic properties were obtained for the doped samples from the magnetic study. The electrical study revealed that the 2% doped sample had the highest conductivity of 1.5 Ωcm^{-1}. Doping of MoO_3 thin films with Cu element has the potential of increasing its conductivity without negatively altering other properties. The deposited films find application in photocells and solar cell devices.

Acknowledgments

ACN (90406558) and FIE (90407830) graciously acknowledge UNISA for Postdoc and VRSP Fellowship awards respectively. We graciously acknowledge the grant by TETFUND under contract number *TETF/DESS/UNN/NSUKKA/STI/VOL.I/B4.33*. We thank the US Army Research Laboratory–Broad Agency Announcement (BAA) for the financial support given to this research (under Contract number W911NF-12-1-0588). Also, we thank Engr. Emeka Okwuosa for the generous sponsorship of April 2014, July 2016 and July 2018 Conference/Workshops on Applications of Nanotechnology to Energy, Health &.Environment conference.

References

[1] A. Bouzidi, N. Benramdane, H. Tabet-Derraz, C. Mathieu, B. Khelifa, R. Desfeux, Effect of substrate temperature on the structural and optical properties of MoO3 thin films prepared by spray pyrolysis technique, Mater. Sci. Eng., B 97 (2003) 5–8, https://doi.org/10.1016/S0921-5107(02)00385-9.
[2] K.S. Rao, K. Ravindranadh, A.K. Kasturi, Structural Stoichiometry and Phase Transitions of MoO 3 Thin Films for Solid State Microbatteries, (2013).
[3] K.A. Gesheva, T. Ivanova, F. Hamelmanna, Optical Coatings of Cvd-Transition Metal Oxides as Functional Layers in "Smart Windows " and X-Ray Mirrors, (2005).
[4] K. Gesheva, A. Szekeres, T. Ivanova, Optical properties of chemical vapor deposited thin films of molybdenum and tungsten based metal oxides, Sol. Energy Mater. Sol. Cells 76 (2003) 563–576, https://doi.org/10.1016/S0927-0248(02)00267-2.
[5] A.K. Prasad, D.J. Kubinski, P.I. Gouma, Comparison of sol–gel and ion beam deposited MoO3 thin film gas sensors for selective ammonia detection, Sens. Actuators B Chem. 93 (2003) 25–30, https://doi.org/10.1016/S0925-4005(03)00336-8.
[6] K. Hosono, I. Matsubara, N. Murayama, S. Woosuck, N. Izu, Synthesis of polypyrrole/MoO3 hybrid thin films and their volatile organic compound gas-sensing properties, Chem. Mater. 17 (2005) 349–354, https://doi.org/10.1021/cm0492641.
[7] W. Li, F. Cheng, Z. Tao, J. Chen, Vapor-transportation preparation and reversible lithium intercalation/deintercalation of α-MoO3 microrods, J. Phys. Chem. B 110 (2006) 119–124, https://doi.org/10.1021/jp0553784.
[8] W. Lu, X. Chen, M. Xue, Y. Cui, Q. Zhuang, Ultrasonic synthesis of α-MoO3 Nanobelt@CNTs composite for lithium battery and its electrochemical performances, Int. J. Electrochem. Sci. 13 (2018) 12.
[9] H.-Y. Chen, H.-C. Su, C.-H. Chen, K.-L. Liu, C.-M. Tsai, S.-J. Yen, T.-R. Yew, Indium-doped molybdenum oxide as a new p-type transparent conductive oxide, J. Mater. Chem. 21 (2011) 5745–5752, https://doi.org/10.1039/C0JM03815F.
[10] V. Bhosle, A. Tiwari, J. Narayan, Epitaxial growth and properties of MoOx(2, J. Appl. Phys. 97 (2005) 083539, , https://doi.org/10.1063/1.1868852.
[11] J. Okumu, F. Koerfer, C. Salinga, M. Wuttig, In situ measurements of thickness changes and mechanical stress upon gasochromic switching of thin MoOx films, J. Appl. Phys. 95 (2004) 7632–7636, https://doi.org/10.1063/1.1728309.
[12] M.B. Rahmani, S.H. Keshmiri, J. Yu, A.Z. Sadek, L. Al-Mashat, A. Moafi, K. Latham, Y.X. Li, W. Wlodarski, K. Kalantar-zadeh, Gas sensing properties of thermally evaporated lamellar MoO3, Sens. Actuators B Chem. 145 (2010) 13–19, https://doi.org/10.1016/j.snb.2009.11.007.
[13] C.H.S.S. Pavan Kumar, R. Pandeeswari, B.G. Jeyaprakash, Structural, morphological and optical properties of spray deposited Mn-doped CeO2 thin films, J. Alloy. Comp. 602 (2014) 180–186, https://doi.org/10.1016/j.jallcom.2014.02.143.
[14] A.C. Nkele, U.K. Chime, A.C. Nwanya, D. Obi, R.U. Osuji, R. Bucher, P.M. Ejikeme, M. Maaza, F.I. Ezema, Role of metallic dopants on the properties of copper (1) iodide nanopod-like structures, Vacuum 161 (2019) 306–313, https://doi.org/10.1016/j.vacuum.2018.12.049.
[15] A.C. Nkele, A.C. Nwanya, U. Nwankwo, A.B.C. Ekwealor, R.U. Osuji, R. Bucher,

M. Maaza, F.I. Ezema, Structural, optical and electrochemical properties of SILAR-deposited zirconium-doped cadmium oxide thin films, Mater. Res. Express (2019), https://doi.org/10.1088/2053-1591/ab31f5.
[16] R.O. Ijeh, A.C. Nwanya, A.C. Nkele, I.G. Madiba, Z. Khumalo, A.K.H. Bashir, R.U. Osuji, M. Maaza, F.I. Ezema, Magnetic and optical properties of electro-deposited nanospherical copper doped nickel oxide thin films, Phys. E Low-dimens. Syst. Nanostruct. 113 (2019) 233–239, https://doi.org/10.1016/j.physe.2019.05.013.
[17] V.D. Phadtare, V.G. Parale, G.K. Kulkarni, H.-H. Park, V.R. Puri, Microwave dielectric properties of barium substituted screen printed CaBi2Nb2O9 ceramic thick films, Ceram. Int. 44 (2018) 7515–7523, https://doi.org/10.1016/j.ceramint.2018.01.150.
[18] R.R. Powar, V.D. Phadtare, V.G. Parale, H.-H. Park, S. Pathak, P.R. Kamble, P.B. Piste, D.N. Zambare, Structural, morphological, and magnetic properties of ZnxCo1-xFe2O4 (0 ≤ x ≤ 1) prepared using a chemical co-precipitation method, Ceram. Int. 44 (2018) 20782–20789, https://doi.org/10.1016/j.ceramint.2018.08.079.
[19] V.D. Phadtare, V.G. Parale, K.-Y. Lee, T. Kim, V.R. Puri, H.-H. Park, Flexible and lightweight Fe3O4/polymer foam composites for microwave-absorption applications, J. Alloy. Comp. 805 (2019) 120–129, https://doi.org/10.1016/j.jallcom.2019.07.048.
[20] Z.-Y. Chen, Y. Chen, Q.K. Zhang, X.Q. Tang, D.D. Wang, Z.Q. Chen, P. Mascher, S.J. Wang, Vacancy-induced ferromagnetic behavior in antiferromagnetic NiO nanoparticles: a positron annihilation study, ECS J. Solid State Sci. Technol. 6 (2017) P798–P804, https://doi.org/10.1149/2.0081712jss.
[21] A. Boukhachem, C. Bouzidi, R. Boughalmi, R. Ouerteni, M. Kahlaoui, B. Ouni, H. Elhouichet, M. Amlouk, Physical investigations on MoO3 sprayed thin film for selective sensitivity applications, Ceram. Int. 40 (2014) 13427–13435, https://doi.org/10.1016/j.ceramint.2014.05.062.
[22] A. Boukhachem, O. Kamoun, C. Mrabet, C. Mannai, N. Zouaghi, A. Yumak, K. Boubaker, M. Amlouk, Structural, optical, vibrational and photoluminescence studies of Sn-doped MoO3 sprayed thin films, Mater. Res. Bull. 72 (2015) 252–263, https://doi.org/10.1016/j.materresbull.2015.08.011.
[23] W. Dong, B. Dunn, Sol–gel synthesis and characterization of molybdenum oxide gels, J. Non-Cryst. Solids 225 (1998) 135–140, https://doi.org/10.1016/S0022-3093(98)00018-0.
[24] Y. Bai, X. Liu, L. Chen, Khizar-ul-Haq, M.A. Khan, W.Q. Zhu, X.Y. Jiang, Z.L. Zhang, Organic thin-film field-effect transistors with MoO3/Al electrode and OTS/SiO2 bilayer gate insulator, Microelectron. J. 38 (2007) 1185–1190, https://doi.org/10.1016/j.mejo.2007.09.010.
[25] Q.-J. Sun, Z. Xu, S.-L. Zhao, F.-J. Zhang, L.-Y. Gao, Y.-S. Wang, The performance improvement in pentacene organic thin film transistors by inserting C60/MoO3 ultrathin layers, Synth. Met. 160 (2010) 2239–2243, https://doi.org/10.1016/j.synthmet.2010.08.007.
[26] A.C. Nkele, A.C. Nwanya, N.U. Nwankwo, R.U. Osuji, A.B.C. Ekwealor, P.M. Ejikeme, M. Maaza, F.I. Ezema, Investigating the properties of nano nest-like nickel oxide and the NiO/Perovskite for potential application as a hole transport material, Adv. Nat. Sci. Nanosci. Nanotechnol. 10 (2019) 045009, , https://doi.org/10.1088/2043-6254/ab5102.
[27] B.N. Ezealigo, A.C. Nwanya, A. Simo, R.U. Osuji, R. Bucher, M. Maaza, F.I. Ezema, Optical and electrochemical capacitive properties of copper (I) iodide thin film deposited by SILAR method, Arabian J. Chem. 12 (8) (2017) 5380–5391.
[28] A.C. Nwanya, D. Obi, K.I. Ozoemena, R.U. Osuji, C. Awada, A. Ruediger, M. Maaza, F. Rosei, F.I. Ezema, Facile synthesis of nanosheet-like CuO film and its potential application as a high-performance pseudocapacitor electrode, Electrochim. Acta 198 (2016) 220–230, https://doi.org/10.1016/j.electacta.2016.03.064.
[29] H. Kermani, H.R. Fallah, M. Hajimahmoodzadeh, Design and fabrication of nanometric ZnS/Ag/MoO3 transparent conductive electrode and investigating the effect of annealing process on its characteristics, Phys. E Low-dimens. Syst. Nanostruct. 47 (2013) 303–308, https://doi.org/10.1016/j.physe.2012.09.031.
[30] N.R. Paudel, A.D. Compaan, Y. Yan, Sputtered CdS/CdTe solar cells with MoO3−x/Au back contacts, Sol. Energy Mater. Sol. Cells 113 (2013) 26–30, https://doi.org/10.1016/j.solmat.2013.01.041.
[31] M. Ghasemi Varnamkhasti, H.R. Fallah, M. Mostajaboddavati, A. Hassanzadeh, Influence of Ag thickness on electrical, optical and structural properties of nanocrystalline MoO3/Ag/ITO multilayer for optoelectronic applications, Vacuum 86 (2012) 1318–1322, https://doi.org/10.1016/j.vacuum.2011.12.002.
[32] L. Chibane, M.S. Belkaid, R. Zirmi, A. Moussi, A simple process for synthesis of transparent thin films of molybdenum trioxide in the orthorhombic phase (α-MoO3), J. Electron. Mater. 46 (2017) 1963–1970, https://doi.org/10.1007/s11664-016-5239-1.
[33] V. Nirupama, M.C. Sekhar, T.K. Subramanyam, S. Uthanna, Structural and electrical characterization of magnetron sputtered MoO3thin films, J. Phys. Conf. Ser. 208 (2010) 012101, , https://doi.org/10.1088/1742-6596/208/1/012101.
[34] S. Subbarayudu, V. Madhavi, S. Uthanna, Growth of MoO 3 films by RF magnetron sputtering: studies on the structural, optical, and electrochromic properties, ISRN Condens. Matter Phys. 2013 (2013) 1–9, https://doi.org/10.1155/2013/806374.
[35] J. Wu, L. Zhang, Y. Wang, Y. Long, H. Gao, X. Zhang, N. Zhao, Y. Cai, J. Xu, Mussel-inspired chemistry for robust and surface-modifiable multilayer films, Langmuir 27 (2011) 13684–13691, https://doi.org/10.1021/la2027237.
[36] Y. Cao, X. Zhang, L. Tao, K. Li, Z. Xue, L. Feng, Y. Wei, Mussel-inspired chemistry and michael addition reaction for efficient oil/water separation, ACS Appl. Mater. Interfaces 5 (2013) 4438–4442, https://doi.org/10.1021/am4008598.
[37] A.C. Sonavane, A.I. Inamdar, P.S. Shinde, H.P. Deshmukh, R.S. Patil, P.S. Patil, Efficient electrochromic nickel oxide thin films by electrodeposition, J. Alloy. Comp. 489 (2010) 667–673, https://doi.org/10.1016/j.jallcom.2009.09.146.
[38] Rosalinda Inguanta, Tiziana Spano, Salvatore Piazza, Carmelo Sunseri, Francesco Barreca, Enza Fazio, Fortunato Neri, Letteria Silipigni, Electrodeposition and characterization of mo oxide nanostructures, Chem. Eng. Trans. 43 (2015) 685–690, https://doi.org/10.3303/CET1543115.
[39] T. He, J. Yao, Photochromism of molybdenum oxide, J. Photochem. Photobiol. C Photochem. Rev. 4 (2003) 125–143, https://doi.org/10.1016/S1389-5567(03)00025-X.
[40] T.F. Paes, A.F. Beloto, E.C. de S. Galvão, L.A. Berni, Simple method for measuring the porosity, thickness and refractive index of porous silicon, based on the Fabry-Pérot interference spectrum, Revista Brasileira de Aplicações de Vácuo 35 (2017) 117–122, https://doi.org/10.17563/rbav.v35i3.1044.
[41] E. Elangovan, A. Marques, A.S. Viana, R. Martins, E. Fortunato, Some studies on highly transparent wide band gap indium molybdenum oxide thin films rf sputtered at room temperature, Thin Solid Films 516 (2008) 1359–1364, https://doi.org/10.1016/j.tsf.2007.03.155.
[42] B.R. Rehani, P.B. Joshi, K.N. Lad, A. Pratap, Crystallite size estimation of elemental and composite silver nano-powders using XRD principles, IJPAP 44 (2006) (02) [February 2006], http://nopr.niscair.res.in/handle/123456789/8253 , Accessed date: 24 April 2019.
[43] R. Kumari, A. Sahai, N. Goswami, Effect of nitrogen doping on structural and optical properties of ZnO nanoparticles, Prog. Nat. Sci.: Mater. Int. 25 (2015) 300–309, https://doi.org/10.1016/j.pnsc.2015.08.003.
[44] A. Sahai, Y. Kumar, V. Agarwal, S.F. Olive-Méndez, N. Goswami, Doping concentration driven morphological evolution of Fe doped ZnO nanostructures, J. Appl. Phys. 116 (2014) 164315, https://doi.org/10.1063/1.4900721.
[45] R. Yousefi, A.K. Zak, F. Jamali-Sheini, Growth, X-ray peak broadening studies, and optical properties of Mg-doped ZnO nanoparticles, Mater. Sci. Semicond. Process. 16 (2013) 771–777, https://doi.org/10.1016/j.mssp.2012.12.025.
[46] K. Yamamoto, R. Shimizu, S. Shiraki, T. Hitosugi, Transparent conducting properties of Re-doped β-MoO3 films, Apl. Mater. 4 (2016) 096104, , https://doi.org/10.1063/1.4963154.
[47] P. Mallick, C. Rath, R. Biswal, N.C. Mishra, Structural and magnetic properties of Fe doped NiO, Indian J. Phys. 83 (2009) 517–523, https://doi.org/10.1007/s12648-009-0012-4.
[48] K.H. Kim, C. Takahashi, T. Okubo, Y. Abe, M. Kawamura, Influence of NiO anode buffer layer prepared by solution on performance of bulk-heterojunction solar cells, Appl. Surf. Sci. 258 (2012) 7809–7812, https://doi.org/10.1016/j.apsusc.2012.04.017.
[49] C. Julien, A. Khelfa, O.M. Hussain, G.A. Nazri, Synthesis and characterization of flash-evaporated MoO3 thin films, J. Cryst. Growth 156 (1995) 235–244, https://doi.org/10.1016/0022-0248(95)00269-3.
[50] M. Ganchev, M. Sendova-Vassileva, G. Popkirov, P. Vitanov, Thermal treatment of solution-processed nano-sized thin films of molybdenum oxide, J. Phys. Conf. Ser. 764 (2016) 012011, , https://doi.org/10.1088/1742-6596/764/1/012011.
[51] V.K. Sabhapathi, O.M. Hussain, S. Uthanna, B.S. Naidu, P.J. Reddy, C. Julien, M. Balkanski, A.c. conductivity studies on Al/MoO3/Al sandwich structures, Mater. Sci. Eng., B 32 (1995) 93–97, https://doi.org/10.1016/0921-5107(94)01173-7.
[52] I. Manouchehri, D. Mehrparvar, R. Moradian, K. Gholami, T. Osati, Investigation of structural and optical properties of copper doped NiO thin films deposited by RF magnetron reactive sputtering, Optik 127 (2016) 8124–8129, https://doi.org/10.1016/j.ijleo.2016.06.005.
[53] S. Uthanna, V. Nirupama, J.F. Pierson, Substrate temperature influenced structural, electrical and optical properties of dc magnetron sputtered MoO3 films, Appl. Surf. Sci. 256 (2010) 3133–3137, https://doi.org/10.1016/j.apsusc.2009.11.086.
[54] C. Reyes-Betanzo, J.L. Herrera-Pérez, G.H. Cocoletzi, O. Zelaya-Angel, Refractive index of colored films of molybdenum trioxide, J. Appl. Phys. 88 (2000) 223–226, https://doi.org/10.1063/1.373646.
[55] R. Cárdenas, J. Torres, J.E. Alfonso, Optical characterization of MoO3 thin films produced by continuous wave CO2 laser-assisted evaporation, Thin Solid Films 478 (2005) 146–151, https://doi.org/10.1016/j.tsf.2004.10.027.
[56] H.s. Bolarinwa, M.u. Onuu, A.y. Fasasi, S.o. Alayande, L.o. Animasahun, I.o. Abdulsalami, O.g. Fadodun, I.a. Egunjobi, Determination of optical parameters of zinc oxide nanofibre deposited by electrospinning technique, J. Taibah Univ. Sci. 11 (2017) 1245–1258, https://doi.org/10.1016/j.jtusci.2017.01.004.
[57] R.V. Barde, Influence of CeO2 content on complex optical parameters of phosphovanadate glass system, Spectrochim. Acta A Mol. Biomol. Spectrosc. 153 (2016) 160–164, https://doi.org/10.1016/j.saa.2015.08.023.
[58] S. Ali, M.A. Farrukh, Effect of calcination temperature on the structural, thermodynamic, and optical properties of MoO3 nanoparticles, J. Chin. Chem. Soc. 65 (2018) 276–288, https://doi.org/10.1002/jccs.201700163.
[59] S. Sriram, A. Thayumanavan, Optical and electrical properties of nitrogen doped zno thin films prepared by low cost spray pyrolysis technique, n.d.
[60] O.O. Apeh, U. Chime, S.N. Agbo, S. Ezugwu, R. Taziwa, E. Meyer, P. Sutta, M. Maaza, F.I. Ezema, Properties of nanostructured ZnO thin films synthesized using a modified aqueous chemical growth method, Mater. Res. Express (2018), https://doi.org/10.1088/2053-1591/aadcd6.
[61] 新井敏弘, T.S. Moss, G.J. Burrell, B. Ellis, Semiconductor Opto-Electronics, Butterworths, London, 1973, pp. 874–875 441ページ, 23×15cm, 8,750円., 日本物理學會誌. 28 (1973) https://ci.nii.ac.jp/naid/110002072832/ , Accessed date: 8 April 2019.
[62] M.E. McHenry, D.E. Laughlin, Nano-scale materials development for future magnetic applications, Acta Mater. 48 (2000) 223–238, https://doi.org/10.1016/S1359-6454(99)00296-7.
[63] S.R. Shinde, S.B. Ogale, J.S. Higgins, H. Zheng, A.J. Millis, V.N. Kulkarni, R. Ramesh, R.L. Greene, T. Venkatesan, Co-occurrence of superparamagnetism and anomalous Hall effect in highly reduced cobalt-doped rutile ${\mathrm{TiO}}_

{2\ensuremath{-}\ensuremath{\delta}}$ films, Phys. Rev. Lett. 92 (2004) 166601, https://doi.org/10.1103/PhysRevLett.92.166601.
[64] S.B. Ogale, R.J. Choudhary, J.P. Buban, S.E. Lofland, S.R. Shinde, S.N. Kale, V.N. Kulkarni, J. Higgins, C. Lanci, J.R. Simpson, N.D. Browning, S. Das Sarma, H.D. Drew, R.L. Greene, T. Venkatesan, High Temperature Ferromagnetism with a Giant Magnetic Moment in Transparent Co-doped ${\mathrm{S}\mathrm{n}\mathrm{O}}_{2\ensuremath{-}\ensuremath{\delta}}$, Phys. Rev. Lett. 91 (2003) 077205, , https://doi.org/10.1103/PhysRevLett.91.077205.
[65] R. Kumar, F. Singh, B. Angadi, J.-W. Choi, W.-K. Choi, K. Jeong, J.-H. Song, M.W. Khan, J.P. Srivastava, A. Kumar, R.P. Tandon, Single phase formation of Co-implanted ZnO thin films by swift heavy ion irradiation: optical studies, J. Appl. Phys. 100 (2006) 113708, https://doi.org/10.1063/1.2399893.
[66] A.H. Shah, M. Basheer Ahamed, E. Manikandan, R. Chandramohan, M. Iydroose, Magnetic, optical and structural studies on Ag doped ZnO nanoparticles, J. Mater. Sci. Mater. Electron. 24 (2013) 2302–2308, https://doi.org/10.1007/s10854-013-1093-6.
[67] N. Gopalakrishnan, L. Balakrishnan, A. Brindha, G. Jayalakshmi, Thickness and substrate orientation dependence of ferromagnetism in Mn doped ZnO thin films, Cryst. Res. Technol. 47 (2012) 45–52, https://doi.org/10.1002/crat.201100425.
[68] A.G. Abraham, A. Manikandan, E. Manikandan, S. Vadivel, S.K. Jaganathan, A. Baykal, P.S. Renganathan, Enhanced magneto-optical and photo-catalytic properties of transition metal cobalt (Co2+ ions) doped spinel MgFe2O4 ferrite nanocomposites, J. Magn. Magn. Mater. 452 (2018) 380–388, https://doi.org/10.1016/j.jmmm.2018.01.001.
[69] S.A. Ahmed, X. Ding, P.P. Murmu, N.N. Bao, R. Liu, J.V. Kennedy, J. Ding, J. Yi, Magnetic properties of Co doped WSe2 by implantation, J. Alloy. Comp. 731 (2018) 25–31, https://doi.org/10.1016/j.jallcom.2017.09.288.
[70] G.S. Zakharova, C. Täschner, V.L. Volkov, I. Hellmann, R. Klingeler, A. Leonhardt, B. Büchner, MoO3 − δ nanorods: synthesis, characterization and magnetic properties, Solid State Sci. 9 (2007) 1028–1032, https://doi.org/10.1016/j.solidstatesciences.2007.07.022.
[71] Y. Singh, Electrical resistivity measurements: a review, Int. J. Mod. Phys. Conf. Ser. 22 (2013) 745–756, https://doi.org/10.1142/S2010194513010970.
[72] E. Muchuweni, T.S. Sathiaraj, H. Nyakotyo, Synthesis and characterization of zinc oxide thin films for optoelectronic applications, Heliyon 3 (2017) e00285, , https://doi.org/10.1016/j.heliyon.2017.e00285.